Topology optimization of the harmonic content for torque ripple minimization

Thomas Gauthey, Maya Hage-Hassan, Frédéric Messine, Frédéric Gillon

Topology optimization of the harmonic content for torque ripple minimization

Thomas Gauthey [1], Maya Hage Hassan [1], Frédéric Messine [2] and Frédéric Gillon [3]
[1]Université Paris-Saclay, CentraleSupélec, Sorbonne Université, CNRS, Group of electrical engineering - Paris, 91192, Gif-sur-Yvette, France, thomas.gauthey@centralesupelec.fr, maya.hage-hassan@centralesupelec.fr
[2] LAPLACE, ENSEEIHT-INPT, Université de Toulouse, Toulouse, France, frederic.messine@laplace.univ-tlse.fr
[3] Univ. Lille, Arts et Metiers Institute of Technology, Centrale Lille, Junia, ULR 2697 - L2EP, Lille, France, frederic.gillon@centralelille.fr

This paper proposes a formulation to minimize the torque ripple of switched reluctance machines by means of topology optimization. The novelty lies in targeting critical harmonics which allows for more control, both in the design of the rotor and the harmonic content of the torque, during the ripple minimization. An efficient gradient-based algorithm is used to solve the optimization problem and the gradient is obtained using the adjoint variable method.

***Index Terms*—Design tools, electrical machines, magnetostatics, topology optimization**

I. Introduction

SWITCHED reluctance machines (SRM) have the advantages of low cost and high stability thanks to their relatively simple structures. In the past decades, they have been considered as potential candidates for electrical and hybrid mobility. For that purpose, several studies [1], [2] have addressed its two main drawbacks: low mean torque and high ripple. These performances are highly linked with the rotor and stator geometries and the current control methods.

In topology optimization literature, several methods have been proposed and applied to the design of switched reluctance motors focusing on the rotor design. In most papers where the ripple is the objective, stochastic algorithms are used [3]. To allow for the use of fast-converging gradient algorithms, this criterion is often replaced by the normalized variance of the torque or its square root as in [4]. More rarely, some authors investigated harmonic-based formulations for ripple minimization. In [5], the authors applied the Solid Isotropic Material with Penalization method (SIMP) to the design of a 6/4 SRM such that the torque profile fits a proposed one. The objective function is formulated as the Fourier series expansion of the inductance. In [6], the authors proposed to use the total harmonic distortion of the electromotive force as the objective function to design the rotor of an electrical machine.

In this paper, we propose to combine both approaches, thus keeping the efficiency of the variance-based method and the fine-tuning capabilities of a harmonic-based method by targeting critical torque harmonics. The constrained problem is solved using the Bound-Constrained Lagrangian Method (BCL) [7], setting an inequality constraint on the minimum mean torque value.

II. Case study and performance evaluation

To evaluate the performances of the case study machine, 2D non-linear magnetostatic problems [1] are solved for determining the potential vector u_k for N rotor positions $(\theta_k)_{0\leq k<N}$ by mean of finite element analysis using the NGPy Python package [8]. Thus, the problem in its weak form (1) can be written as:

$$\text{Find } u_k,\ \underbrace{\int_\Omega \nu(\rho,|\nabla u_k|)\nabla u_k \nabla v_k\, dx}_{K_{\theta_k}(u_k,v_k,\rho)} = \underbrace{\int_\Omega j(\theta_k)\, v_k\, dx}_{f_{\theta_k}(v_k)},\quad \forall v_k \tag{1}$$

where v_k are the shape functions hereafter chosen from P1 conforming piece-wise linear space and ν a domain-wise reluctivity function defined in (2).

$$\nu(\rho,|\nabla u|) = \begin{cases} \nu_0 + f(\rho)(\hat{\nu}(|\nabla u|) - \nu_0) & \text{in } \Omega_{rotor} \\ \hat{\nu}(|\nabla u|) & \text{in } \Omega_{stator} \\ \nu_0 & \text{in } \Omega_{air,axis,coils} \end{cases} \tag{2}$$

The non-linear behavior of the ferromagnetic material $\hat{\nu}$ is modeled using the Marrocco BH-curve approximation [9]. The material curve proposed Fig.1 is similar to M-19 steel, with a saturation point around 1.8 T.

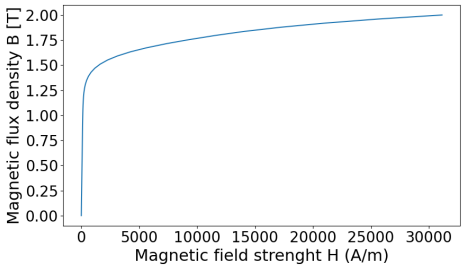

Fig. 1: Ferromagnetic material properties: BH curve

In the rotor design domain, a scalar density field ρ is defined as the design variable of the topology optimization problem. For the interpolation function $f(\rho)$ (Fig.2), a SIMP-All [10] formulation like the one proposed in [11] is chosen. Thus,

$$f(\rho) = \frac{2\nu_0}{\nu_{iron}+\nu_0}\rho - \frac{\nu_0-\nu_{iron}}{\nu_{iron}+\nu_0}\rho^2 \tag{3}$$

Corresponding author: T. Gauthey (email: thomas.gauthey@centralesupelec.fr).

where $\nu_{iron} = \nu_0/6356$ is the equivalent reluctivity for low excitation, i.e., in the linear part of the BH-curve.

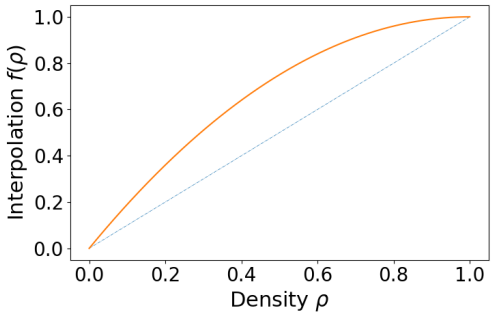

Fig. 2: Interpolation function $f(\rho)$

For our study, we choose a benchmark SRM, as shown in Fig.3, with four stator teeth like the one presented in [12] and optimized by a parametric approach.

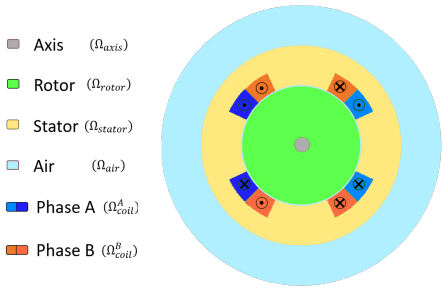

Fig. 3: Case study geometry

With this simple geometry and steps $j(\theta)$ for current shaping, the machine exhibits the two main drawbacks of this machine type for classical rotor design [12]. The dimensions and current parameters are given in Table.I.

TABLE I: Geometric and winding parameters

Parameter	Value	Unit
Axis radius	5	mm
Rotor radius	29.5	mm
Air gap width	0.5	mm
Inner stator radius	30	mm
Outer coil radius	40	mm
Outer stator radius	50	mm
Air boundary radius	70	mm
Stator tooth angle	50	°
Length L_z	120	mm
Maximum current density J_{max}	5	A/mm²
Number of pole pairs	1	-

The instantaneous torques T_k are uniformly sampled for $N = 180$ mechanical angular positions θ_k between 0 and $\pi/2$. They are computed using Arkkio's method [13] integrating Maxwell's stress tensor over a band of a few mesh elements inside the gap. The rotation of the rotor is considered using the Moving Band Method [14]. Thus, for a vector $\mathbf{T}$ of instantaneous torque, the norm of the mth harmonic can be computed using the discrete Fourier transform, such as :

$$\mathrm{DFT}(\mathbf{T})[m] = \frac{2}{N}\left|\sum_{i=0}^{N-1}\left(\cos\left(\theta_{m,i}\right) + \mathbf{j}\sin\left(\theta_{m,i}\right)\right)T_i\right|. \quad (4)$$

Hence for a simple design obtained by a preliminary mean torque maximization problem, we get the following design Fig.4 and associated harmonic content. As the BCL method requires an initial point that satisfies the constraints, this design will be used as such for all problems presented below.

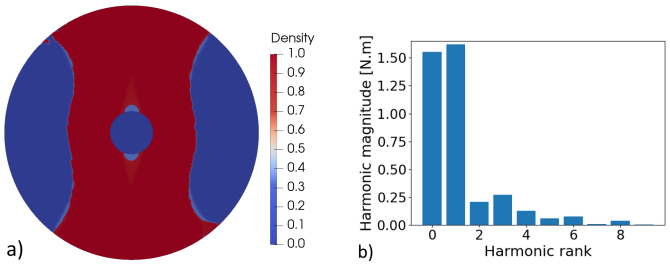

Fig. 4: Mean torque maximization a) rotor design and b) harmonic content

Here, the primary source of the ripple is the first harmonic over the mechanical angular range [0,$\pi/2$], which stems from the interactions between the four stator teeth and the two teeth of the rotor. We choose to focus on this specific harmonic as it is the main source of vibration and noise [15].

III. Optimization Problem

The problem of minimization of the m^{th} harmonic under a constraint on the minimum value of the mean torque can be formulated as follows:

$$(\mathcal{P}_m): \begin{cases} \min\limits_{\rho} \mathrm{DFT}(\mathbf{T})[m] \\ u.c.\ K_{\theta_k}(u_k, v_k, \rho) = f_{\theta_k}(v_k)\ \forall\, v_k, \forall k \\ u.c.\ \bar{\mathbf{T}} \geq \bar{T}_{min} (= 1.5\ \mathrm{N.m}) \end{cases}. \quad (5)$$

We compute the gradient by searching for a saddle point of the associated Lagrangian operator $\mathcal{L}$ using the adjoint variable method to get a descent direction.

$$\begin{aligned}\mathcal{L}(\mathbf{U}, \mathbf{\Lambda}, \rho) = \mathrm{DFT}(\mathbf{T})[m] + \psi(\bar{\mathbf{T}} - \bar{T}_{min}, \lambda^*, \mu) \\ + \sum_{k=0}^{N-1}\left(K_{\theta_k}(u_k, \lambda_k, \rho) - f_{\theta_k}(\lambda_k)\right)\end{aligned} \quad (6)$$

where $\mathbf{U} = [u_k, k \in [\![0, N-1]\!]]$ is the vector of state, $\Lambda = [\lambda_k, k \in [\![0, N-1]\!]]$, the vector of adjoint and ψ the function

$$\psi(x, \lambda^*, \mu) = \begin{cases} -\lambda^* x + \frac{\mu}{2}x^2 \\ -\frac{1}{2\mu}(\lambda^*)^2 \end{cases} \quad (7)$$

to handle the inequality constraints where λ^* and μ are multipliers updated according to the Bound-constrained Lagrangian method [7]. Each adjoint λ_k is computed by solving the linear PDE, here written in its weak form:

$$\begin{aligned}\partial_{u_k} K_{\theta_k}(u_k, \lambda_k, \rho)(v_k) = -\partial_{u_k}\mathrm{DFT}(\mathbf{T})[m](v_k) \\ - \partial_{u_k}\psi(\bar{\mathbf{T}} - \bar{T}_{min}, \lambda^*, \mu)(v_k).\end{aligned} \quad (8)$$

To compute the partial derivatives of the K_{θ_k} operator and DFT, the following assumptions are made:

- Magnetic states obtained are all independent of one another as eddy currents are neglected

- For an angular position θ_k, the instantaneous torque T_k is only dependant on the state u_k (i.e. $T_k = T(u_k)$)

Thus, adjoint states are independent of each other and we get the following formulas:

$$\begin{cases} \partial_{u_k} K_{\theta_k}(u_k, \lambda_k, \rho)(v_k) = \int_\Omega \mathcal{A}(\rho, u_k)\nabla\lambda_k \nabla v_k \, \mathrm{d}x \\ \partial_{u_k} \mathrm{DFT}(\mathbf{T})[m](v_k) = \beta_{m,k}(\mathbf{U})\partial_{u_k} T(u_k)(v_k) \end{cases} \tag{9}$$

where $\mathcal{A}(\rho, u_k) = \nu(\rho, |\nabla u_k|) + \frac{\nu'(\rho, |\nabla u_k|)}{|\nabla u_k|}\nabla u_k \otimes \nabla u_k$. The scalar $\beta_{m,k}(\mathbf{U})$ obtained from the chain rule can be written :

$$\beta_{m,k}(\mathbf{U}) = \frac{4\sum_{i=0}^{N-1} cos\left(\frac{2\pi m(i-k)}{N}\right) T(u_i)}{N^2 \, \mathrm{DFT}(\mathbf{T})[m]} \tag{10}$$

Thus, for the right state and adjoint pairs (u_k, λ_k) the sensitivity of the problem can be written (11) as:

$$d_\rho \mathcal{L} = \sum_{k=0}^{N-1} \partial_\rho K_{\theta_k}(u_k, \lambda_k, \rho). \tag{11}$$

We validate our gradient approach by comparing it to the finite difference method. This yields a relative error less than $2.10^{-4}\%$ for tests on uniformly sampled mesh elements

IV. Results and Discussion

In this section, the results from the first harmonic minimization problem are presented and its performances are compared to the literature standard which is the variance minimization. A third hybrid formulation is then presented, harnessing the capabilities of both approaches.

A. Minimization of the first torque harmonic

We solve $(\mathcal{P}_1)$ for the density distribution ρ starting from the design shown in Fig.4. The algorithm reaches its minimal relative improvement stopping criteria ($< 10^{-4}$ in a step) after 52 iterations. A post-processing threshold at $\rho_{th} = 0.75$ is then applied and the algorithm is launched again which converges this time in less than 5 iterations, to correct for inaccuracies and the small performance loss created by the projection. The final design Fig.5 is anti-symmetric due to the fact that only clockwise rotation is considered.

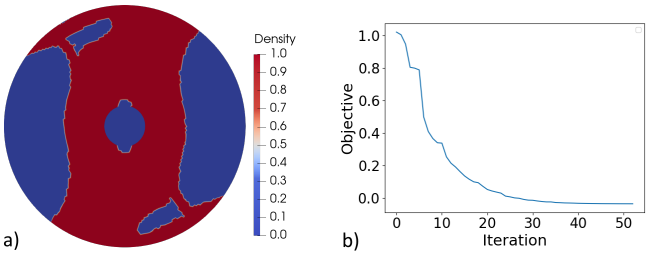

Fig. 5: Optimization results for $\mathcal{P}_1$: a) rotor design and b) convergence curve

The torque ripple Fig.6 is minimized by optimizing the first harmonic from 184% for the initial design to 138% in the final design.

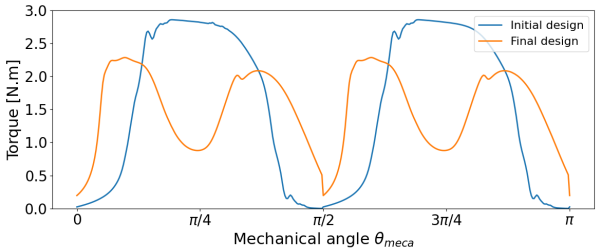

Fig. 6: Compared torque curves

As for the harmonic content, at the end of the optimization procedure, the norm of the first harmonic (highlighted in orange in Fig.7) is reduced to 1/25 of its initial value. However, an expected increase in higher harmonics is observed as the optimization is done for a fixed stator and current-shaping.

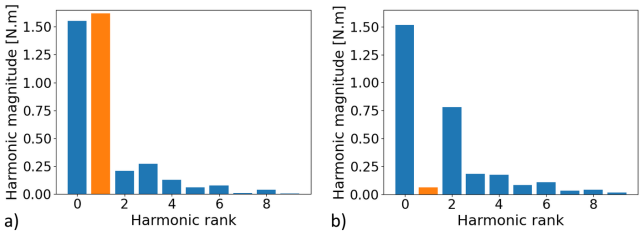

Fig. 7: Compared torque harmonic content for a) the initial design and b) the optimized design

By creating those two holes, the optimizer perturbs the preferred flux path Fig.8 for $\theta_k \approx \pi/4$, thus lowering the torque and cutting the first harmonic.

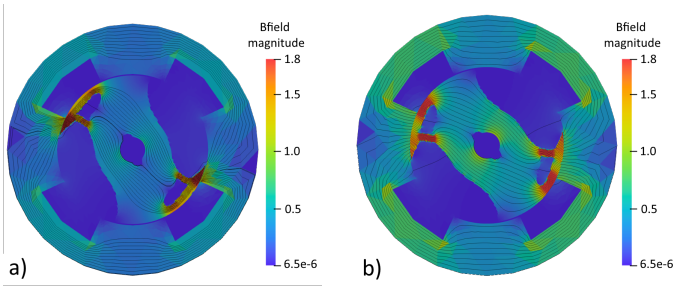

Fig. 8: Flux lines and B-field magnitude for the optimized design at a) $\theta_{meca} = \pi/8$ and b) $\theta_{meca} = \pi/4$

B. Minimization of the RMS torque ripple

In density-based topology optimization, the criteria used for torque ripple minimization is the RMS ripple. This problem is formulated in (12) and solved by the above procedure.

$$(\mathcal{P}_{RMS}) : \begin{cases} \min_\rho \Delta_{RMS}\mathbf{T} \left(= \sqrt{\sum_{i=0}^{N-1} \left(\frac{1}{\bar{T}}\left(T(u_i) - \bar{T}\right)\right)^2} \right) \\ u.c.\ K_{\theta_k}(u_k, v_k, \rho) = f_{\theta_k}(v_k)\ \forall\, v_k, \forall k \\ u.c.\ \bar{\mathbf{T}} \geq \bar{T}_{min} (= 1.5 \text{ N.m}) \end{cases} \tag{12}$$

The final design Fig.9 still is anti-symmetric but with a more complex pattern of holes and differences in bridge widths. The objective function does not discriminate between the different harmonics; they are thus of similar magnitude in the final design. With this design, the ripple is reduced to 83%.

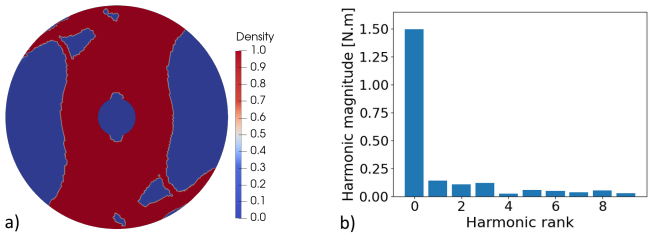

Fig. 9: Optimization results for $\mathcal{P}_{RMS}$: a) rotor design and b) torque harmonic content

C. Simultaneous optimization of the first torque harmonic and RMS ripple

As the RMS ripple and the harmonic are of the same order of magnitude, they can be added without normalization in a combined optimization problem. Here, we prioritize minimizing the ripple being weighting it with a factor of 0.6.

$$(\mathcal{P}_{1,\text{RMS}}): \begin{cases} \min\limits_{\rho} 0.4 \cdot \text{DFT}(\mathbf{T})[m] + 0.6 \cdot \Delta_{RMS}\mathbf{T} \\ u.c.\ K_{\theta_k}(u_k, v_k, \rho) = f_{\theta_k}(v_k)\ \forall\, v_k, \forall k \\ u.c.\ \bar{\mathbf{T}} \geq \bar{T}_{min} (= 1.5\ \text{N.m}) \end{cases} . \quad (13)$$

The final design Fig.10 presents the same characteristics as both previous optimization results keeping the bridge width from the RMS design and the number of holes from the harmonic design.

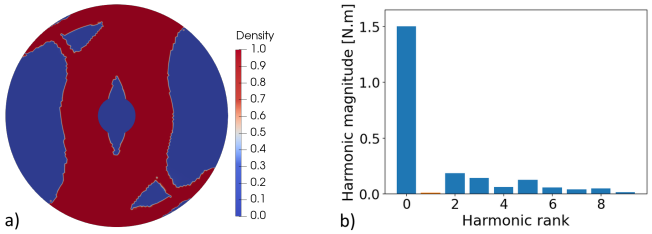

Fig. 10: Optimization results for $\mathcal{P}_{1,RMS}$: a) rotor design and b) torque harmonic content

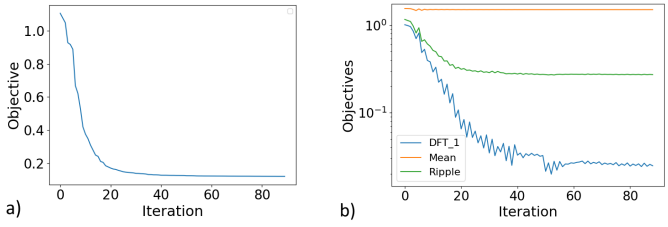

Fig. 11: Convergence curves for $\mathcal{P}_{1,RMS}$: a) Aggregated merit function and b) separated objective and constraints

The first harmonic is reduced to less than a $1/100^{th}$ of its original value, while the ripple is reduced to 83% (Fig. 11).

Computation was done on Intel i9-12900H, 14 cores Laptop, each step taking an average 200s to be processed, mostly taken by 180 non-linear state computations. Thus, with this formulation, the ripple can be optimized while keeping some control over the harmonic content of the torque.

V. Conclusion

In this paper, a formulation for ripple minimization using topology optimization was proposed using the reduction of the harmonic content of the torque and applied the design of the rotor of an SRM. The final design presents an asymmetry due to the rotation direction and holes diverting the flux to limit the ripple. Those may cause mechanical unbalances or stress concentration points. Those will be addressed in a further study along with manufacturability constraints.

Acknowledgment

This work is funded by the GdR SEEDS of the French National Centre for Scientific Research (CNRS).

References

[1] T. Labbe and B. Dehez, "Convexity-oriented method for the topology optimization of ferromagnetic moving parts in electromagnetic actuators using magnetic energy," *IEEE Transactions on Magnetics*, vol. 46, no. 12, pp. 4016–4022, 2010.

[2] O. Brun, O. Chadebec, P. Ferrouillat, I. Niyonzima, J. Siau, G. Meunier, *et al.*, "Sensitivity analysis using the virtual work principle for 2-d magnetostatic problems," *IEEE Transactions on Magnetics*, vol. 59, no. 5, pp. 1–4, 2023.

[3] Y. Otomo, H. Igarashi, T. Sato, Y. Suetsugu, and E. Fujioka, "2.5-d multi-phase topology optimization of permanent magnet motor using gaussian basis function," *IEEE Transactions on Magnetics*, vol. 58, no. 9, pp. 1–4, 2022.

[4] Y. Okamoto, R. Hoshino, S. Wakao, and T. Tsuburaya, "Improvement of torque characteristics for a synchronous reluctance motor using MMA-based topology optimization method," *IEEE Transactions on Magnetics*, vol. 54, no. 3, pp. 1–4, 2018.

[5] J. Lee, J. H. Seo, and N. Kikuchi, "Topology optimization of switched reluctance motors for the desired torque profile," *Structural and Multidisciplinary Optimization*, vol. 42, no. 5, pp. 783–796, 2010.

[6] M. Merkel, P. Gangl, and S. Schöps, "Shape optimization of rotating electric machines using isogeometric analysis," *IEEE Transactions on Energy Conversion*, vol. 36, no. 4, pp. 2683–2690, 2021.

[7] N. Jorge and W. Stephen J, "Penalty, barrier, and augmented lagrangian methods," in *Springer Series in Operations Research and Financial Engineering*, pp. 488–525, Springer-Verlag, 1999.

[8] J. Schoeberl, "C++11 implementation of finite elements in ngsolve," tech. rep., TU Wien, 2014.

[9] A. Marrocco, "Analyse numérique de problèmes d'électrotechnique," *Ann. Sc. Math. Québec*, vol. 1, no. 2, pp. 271–296, 1977.

[10] A. Ferrer, "SIMP-ALL: A generalized SIMP method based on the topological derivative concept," *International Journal for Numerical Methods in Engineering*, vol. 120, no. 3, pp. 361–381, 2019.

[11] T. Gauthey, P. Gangl, and M. H. Hassan, "Multi-material topology optimization with continuous magnetization direction for motors design," in *2022 International Conference on Electrical Machines (ICEM)*, IEEE, Sept. 2022.

[12] P. T. Hieu, D.-H. Lee, and J.-W. Ahn, "Design of a high speed 4/2 switched reluctance motor for blender application," in *2017 IEEE Transportation Electrification Conference and Expo, Asia-Pacific (ITEC Asia-Pacific)*, pp. 1–5, 2017.

[13] A. Arkkio, "Time stepping finite element analysis of induction motors," in *1988 International Conference on Electrical Machines (ICEM)*, 1988.

[14] B. Davat, Z. Ren, and M. Lajoie-Mazenc, "The movement in field modeling," *IEEE Transactions on Magnetics*, vol. 21, no. 6, pp. 2296–2298, 1985.

[15] M. Abdalmagid, E. Sayed, M. H. Bakr, and A. Emadi, "Geometry and topology optimization of switched reluctance machines: A review," *IEEE Access*, vol. 10, pp. 5141–5170, 2022.